Hierarchical Bayesian Optimization of Spatiotemporal Neurostimulations for Targeted Motor Outputs

Samuel Laferrière, Marco Bonizzato, Sandrine L. Côté, Numa Dancause, and Guillaume Lajoie

***Abstract*— The development of neurostimulation techniques to evoke motor patterns is an active area of research. It serves as a crucial experimental tool to probe computation in neural circuits, and has applications in neuroprostheses used to aid recovery of motor function after stroke or injury to the nervous system. There are two important challenges when designing algorithms to unveil and control neurostimulation-to-motor correspondences, thereby linking spatiotemporal patterns of neural stimulation to muscle activation: (1) the exploration of motor maps needs to be fast and efficient (exhaustive search is to be avoided for clinical and experimental reasons) (2) online learning needs to be flexible enough to deal with noise and occasional spurious responses. We propose a stimulation search algorithm to address these issues, and demonstrate its efficacy with experiments in the motor cortex (M1) of a non-human primate model. Our solution is a novel iterative process using Bayesian Optimization via Gaussian Processes on a hierarchy of increasingly complex signal spaces. We show that our algorithm can successfully and rapidly learn correspondences between complex stimulation patterns and evoked muscle activation patterns, where standard approaches fail. Importantly, we uncover nonlinear circuit-level computations in M1 that would have been difficult to identify using conventional mapping techniques.**

***Index Terms*— Neural engineering, machine learning algorithms, optimization methods, motor cortex (M1), neural stimulation.**

Manuscript received October 3, 2019; revised January 7, 2020 and February 29, 2020; accepted March 9, 2020. Date of publication April 9, 2020; date of current version June 5, 2020. The work of Marco Bonizzato was supported by an IVADO Fellowship. The work of Numa Dancause was supported by the FRQNT under Grant 2019- PR-253402. The work of Guillaume Lajoie was supported in part by the NSERC Discovery under Grant RGPIN-2018-04821, in part by the FRQNT Young Investigator under Grant 2019-NC-253251, and in part by the FRQS Research Scholar Award, Junior 1, under Grant LAJGU0401- 253188. *(Corresponding author: Guillaume Lajoie.)*

Samuel Laferrière is with the Computer Science Department, Université de Montréal, Montreal, QC H3T 1N8, Canada, and also with Mila-Quebec AI Institute, Montreal, QC H2S 3H1, Canada.

Marco Bonizzato is with the Neuroscience Department, Université de Montréal, Montreal, QC H3T 1N8, Canada, and also with the CIUSSS NIM-Sacré-Coeur Hospital, Montreal, QC H4J 1C5, Canada.

Sandrine L. Côté, and Numa Dancause are with the Neuroscience Department, Université de Montréal, Montreal, QC H3T 1N8, Canada.

Guillaume Lajoie is with the Mathematics and Statistics Department, Université de Montréal, Montreal, QC H3T 1N8, Canada, and also with Mila-Quebec AI Institute, Montreal, QC H2S 3H1, Canada. (e-mail: g.lajoie@umontreal.ca).

This article has supplementary downloadable material available at http://ieeexplore.ieee.org, provided by the authors.

Digital Object Identifier 10.1109/TNSRE.2020.2987001

I. Introduction

EACH year, over 15 million people worldwide suffer major debilitating motor system injuries such as spinal cord trauma [1] or stroke [2]. A promising approach to help restore movement applies targeted, artificial stimulation to motor structures of the nervous system, e.g. motor cortex [3], spinal cord [4], or the periphery [5] using brain-computer interfaces (BCI). Despite years of research, it is still not fully understood how complex movements are generated [6]–[8], and even less so how to regain control of these movements after injury. Nevertheless, there are often local spatial correspondences between neurostimulation of specific sites and targeted muscle activation, and it is desirable to leverage these in an optimal way. Previous work has shown that long-train stimulation in motor cortex can activate entire circuits of neurons, thereby producing complex movements [6], [7]. However, it is difficult to predict which muscles will be activated in such a scenario. In contrast, the challenge we address here is to specifically identify optimal stimulation signals to evoke *targeted* muscle co-activations, where pre-selected muscles are required to be activated at specific times.

New implantable devices which are microfabricated with many electrodes hold potential for such targeted spatiotemporal stimulation. Yet, existing control algorithms do not fully take advantage of them, generally relying on incomplete and manual mapping, and often on single electrode stimulation. Our goal is to develop Bayesian optimization methods to learn optimal multi-electrode stimulation. Effectively searching the space of possible spatiotemporal stimulation patterns (which can include duration, intensity, location, temporal ordering, etc.) is a complex task because of its combinatorial explosion in size. Exhaustive search is therefore impossible in practice, especially if algorithms are to be used on-line in clinical settings. Moreover, relationships between stimulation and output are noisy, and may change over time due to plasticity of neural circuits [8], [9]. Any method to identify stimulation protocols must be robust, and flexible enough to track such changes.

We propose a Gaussian Process (GP) based Bayesian Optimization (BO) approach[1] that leverages acquired knowledge of muscle responses evoked by stimulation of single channels

[1]We make the data and some example code available at https://github.com/samlaf/hierarchical-gaussian-process.

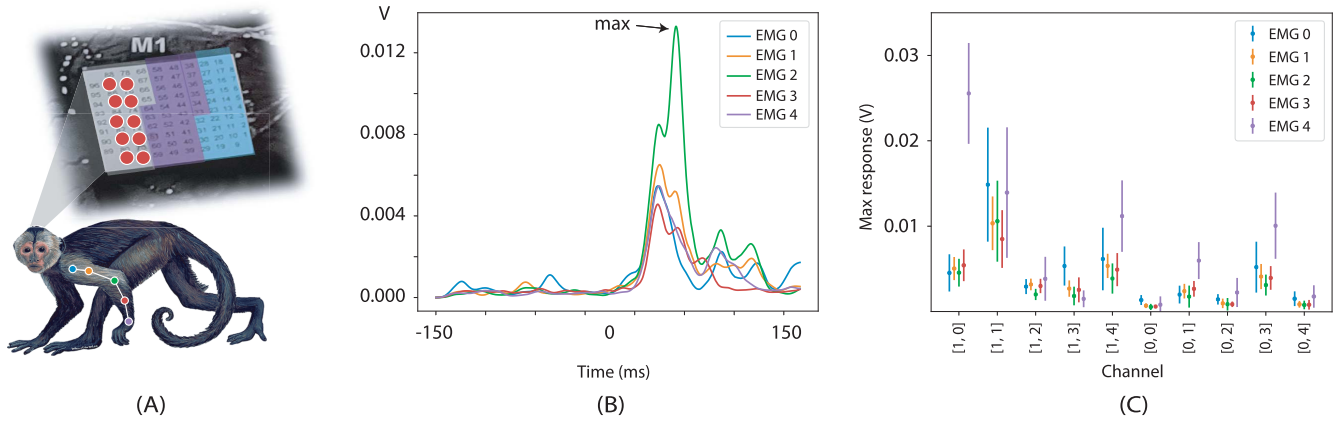

Fig. 1. (A) *Cebus apella* with Utah Array (M1) and implanted muscles (not real locations). Stimulation search space restricted to 2×5 grid in red. (B) EMG responses (rectified) evoked from a single train delivered to a single-channel [1,1]. Arrow shows the max of EMG 2 corresponding to $C(r_2([1,1])) \approx 0.013$. (C) Max response (mean±std) per channel for different muscles. Sample size $n = 10$ for each channel.

to build first order *stim-to-muscle* maps. These are then used as linear *priors* for GP models of multi-channel stimulation patterns, where only nonlinear correction terms need to be learned. We refer to this process as *hierarchical* GP-BO since it relies on GP models fitted in lower dimensional spaces to initialize and constrain ones in higher dimensional spaces, where sampling would be prohibitively costly. The advantages of recursively learning correction terms, rather than a complete map, are threefold: **(1)** Convergence to optimal stimulation requires fewer exploratory stimuli than direct optimization on the space of all signals. **(2)** The algorithm can be used online and adapts quickly to changes in neural dynamics. **(3)** Our method precisely learns the nonlinearities introduced by network dynamics, and can track the evolution of population codes throughout recovery, thus uncovering circuit-level computations.

The main goal of this paper is to describe this novel algorithm applied to stimulation patterns of intracortical microstimulation (ICMS), for targeted patterns of electromyography (EMG) activations. To complement this algorithmic contribution, we demonstrate its efficacy with a basic experiment in a non-human primate model where optimal multi-electrode stimulation patterns are identified to evoke selected muscle coactivations. This experiment is intended as a proof-of-concept for our algorithm and as such, uses a single monkey but validates our findings with multiple combinations of EMG output patterns. For completeness, we record exhaustive spatiotemporal stimulation pattern combinations and their responses on several trials for a selected collection of electrodes and EMGs. We then perform explicit validation of our approach, with offline tests that are run several times. This exhaustive dataset is limited in spatial and temporal resolution because of experimental constraints, but our algorithm is designed to be scaled up towards our goal of evoking even more complex targeted EMG patterns.

In the discussion, we outline the implementation and future use of our algorithm in online settings as well as the circuit-level neural mechanisms present in M1 that it uncovers.

II. Methods

A. Neural Stimulation: Setup and Experiment Description

Experiments were conducted in a male adult capuchin monkey (3 yo) during a single recording session. The experimental protocol followed the guidelines of the Canadian Council on Animal Care and was approved by the *Comité de Déontologie de l'Expérimentation sur les Animaux of the Université de Montréal*. The monkey was food restricted approximately 12h prior to the recording session, and otherwise group housed and supplied with food and water *ad libitum*. Prior to the onset of data collection, a 96-channel microelectrode Utah array was implanted in primary motor cortex (M1) and five different muscles of the forearm and hand were chronically implanted to record EMG activity: *flexor carpi ulnaris, extensor digitorum communis, extensor carpi radialis, opponens pollicis and flexor pollicis brevis* (see illustration in Fig. 1A.[2]) During the recording session, M1 was stimulated by sending electrical pulse trains through one or many channels, and EMG responses we recorded (eg. Fig. 1B). Our goal was to find the optimal stimulation pattern, among a parametric family described below, that evoked a given target EMG response with maximal amplitude.

Mathematically, we consider electrical stimulation signals that are composed of discrete events (single electrical pulses or short pulse trains) that we call *(stimulation) events* for generality. In this article, data collection is restricted to a small 2×5 electrode sub-grid to allow extensive search of a two-electrode stimulation space, formally defined in Sec. III-C. This allows exhaustive measurement of stimulation-to-EMG maps, and provides ground truth comparison for our algorithm. The electrodes used in the search are marked by red dots in Fig. 1A. Stimulation events are chosen to be trains of 13 pulses of 30μA that last 0.2ms each, delivered at 330Hz (for a rough total of 40 ms). Note that the spatial configuration of channels is important for learning as Gaussian Processes make use of this information in their kernel distance function.

[2]Royalty-free image from unixtitan.net

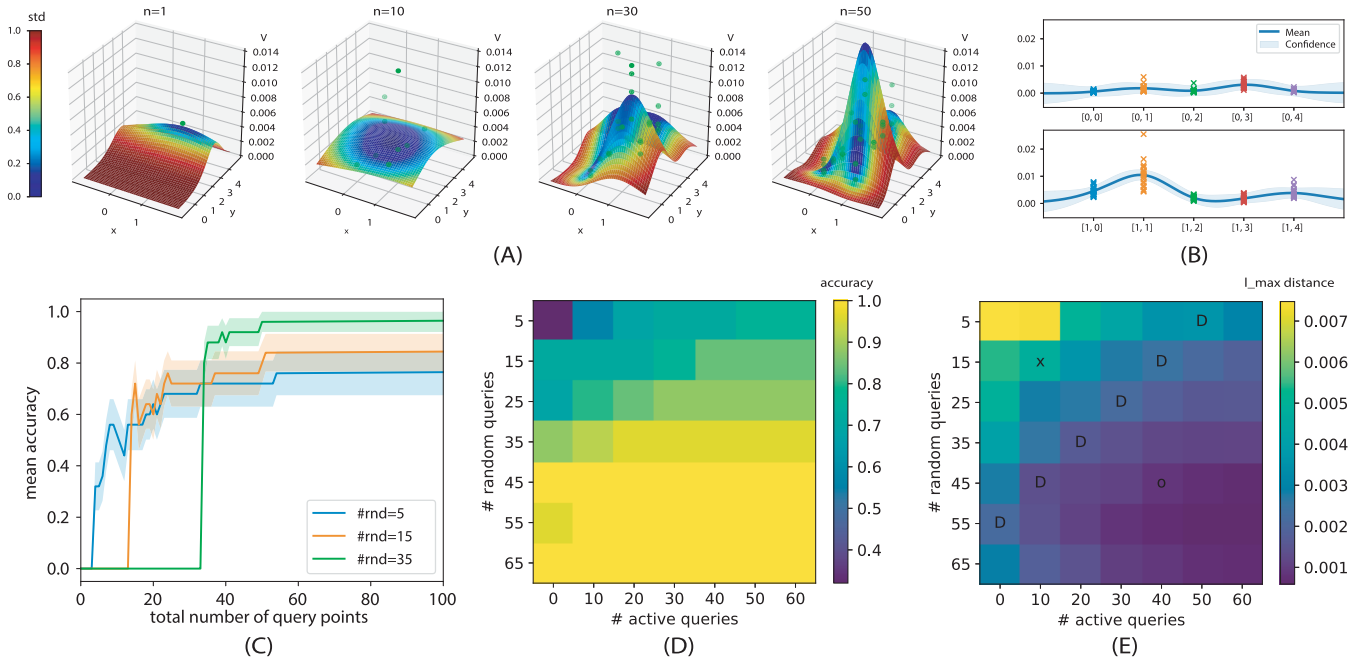

Fig. 2. (A) Gaussian Process fit for activation of EMG-0 for single stimulation event with increasing number of query points shown in green. Surface shows GP's mean $\bar{f}$, and color shows standard deviation. (B) One-dimensional slices of GP (as pictured in A) along the x-coordinates. Markers indicate query responses, blue line indicates GP mean, shaded area is one standard deviation. (C) Mean prediction accuracy for EMG-0 (sampled over 25 separate fits) as a function of total number of queries, for different numbers of initial random queries. Shaded area indicates one standard deviation. (D) Mean prediction accuracy for EMG-0 as a function of number of initial random queries and number of active queries. (E) Distance to optimal solution for single-event GP model on EMG-0. Same data as in D, see text for distance definition. Markers indicate total number of query points: "X"= 25, "D"= 55, "O"= 85.

With this current setup, the data collection protocol takes about an hour, during which the monkey needs to receive ketamine intravenously every 8 minutes.

Each stimulation channel is denoted by discrete Cartesian coordinates $c = [x, y]$, $x \in \{0, 1\}$, $y \in \{0, \ldots, 4\}$ (see Fig. 2A). A stimulation containing k events is a tuple $s_k = (c_1, \Delta t_1, c_2, \ldots, c_{k-1}, \Delta t_{k-1}, c_k,)$ where c_i indicates the channel of the i^{th} event, and Δt_i is the inter-event interval between events i and $i+1$. In this experiment, fixed intensity are used but power could be added to the stimulation parameters with the same formalism (see Discussion). Each s_k generates a noisy response pattern $r(s_k)$. In our case, the (rectified) EMG responses of five muscles are considered: $r(s_k) = (r_0(s_k), \ldots, r_4(s_k))$. The goal is to optimize an objective function $C(r(s_k))$. Here C is flexible; it can be extracting the maximum output of a single EMG response (or combinations of EMG responses), or measuring a distance between the evoked pattern $r(s_k)$ and a target pattern r_{target}. In our case, $C(r(s_k))$ is chosen to return the maximum output of a single $r_i(s_k)$, or combinations of $r_i(s_k)$ for muscle co-activations (see Results), in a window of 150ms following the first stimulus delivery. We want to find

$$\arg\max_{s_k} \mathbb{E}[C(r(s_k))]$$

where the expectation is needed because muscle responses are stochastic. The argmax can be replaced by argmin if we want to minimize a distance function instead of maximizing an amplitude. In this article, we demonstrate and test our algorithm offline on the space of double-event stimulation patterns s_2 (pairs of electrode) for each of $\Delta t = 0, 10, 20, 40, 60, 80, 100$ ms. The EMG responses of each stimulation pattern were recorded over 10 trials each. An online demonstration will be presented in a forthcoming publication.

Importantly, we note that in general $r(s_k)$ could also depend on time, and C could measure different attributes of EMG responses, such as temporally integrated activation or other signal features. Our algorithm can easily be implemented with the experimenter's choice of objective function, as long as it can be expressed as a scalar to be optimized. Our use of $r(s_k)$ (maximal EMG response over a time window) was chosen for its simplicity and effectiveness in capturing muscle activation, for illustrative purposes.

B. Gaussian Processes for Bayesian Optimization

Given the constraints of our problem, namely those of black-box derivative-free global optimization under query limits, Bayesian optimization [10] makes for a natural fit. BO provides uncertainty estimates that allow tracking, and adapting online to, signal delivery changes caused by the implant moving, structural changes in the underlying brain substrate, and muscle response changes due to fatigue.

BO constructs, at every iteration, a probabilistic surrogate to the function C being optimized, which is used to balance exploration and exploitation through the design of an acquisition function. It does so by treating the unknown function C as a random function and placing a prior over it. This

prior dictates attributes of the function such as smoothness and frequency of oscillation. By conditioning on the so far observed responses of the function, a posterior distribution over possible functions is obtained, from which the algorithm can decide where to query next based on optimizing an acquisition function. Acquisition functions convert a probabilistic belief into a deterministic function that explicitly embodies a trade-off between exploration and exploitation. Following the current literature, we choose to model the random surrogate as a Gaussian Process [11], and use the *Upper Confidence Bound* [10] as acquisition function.

1) Gaussian Process Prediction: GPs are such that for a finite number of training data points $\boldsymbol{x}$ and their associated responses $\boldsymbol{y}$ (represented by the plate notation in Appendix Fig. 5), plus a finite number of test data points $\boldsymbol{x}_*$ whose response $\boldsymbol{f}_*$ we would like to predict, we get a Multivariate Gaussian

$$\begin{pmatrix} y \\ f_* \end{pmatrix} \sim \mathcal{N}\left(\begin{pmatrix} m(x) \\ m(x_*) \end{pmatrix}, \begin{pmatrix} K_y(x,x) & K(x,x_*) \\ K(x_*,x) & K(x_*,x_*) \end{pmatrix}\right)$$

where m and K are the mean and kernel functions associated to the GP, and

$$K_y(x_p, x_q) = K(x_p, x_q) + \sigma \mathbb{1}_{x_p = x_q} \tag{1}$$

where σ is the noise standard deviation parameter, which will be optimized along with K's parameters. The prediction for $\boldsymbol{f}_*$ results by simple conditioning of this Multivariate Normal distribution [11]:

$$\begin{aligned} &f_*|x_*, y, x \sim \mathcal{N}\left(\bar{f}_*, \mathrm{cov}(f_*)\right), \text{where} \\ &\bar{f}_* = m(x_*) + K(x_*, x)[K(x,x) + \sigma^2 \boldsymbol{I}]^{-1}(y - m(x)) \\ &\mathrm{cov}(f_*) = K(x_*, x_*) - K(x_*, x)[K(x,x) + \sigma^2 \boldsymbol{I}]^{-1} K(x, x_*). \end{aligned}$$

2) Practical Example: Fig. 1C shows all of the single stimulation event data, where individual EMG responses to single events are considered. Note that different EMGs can have different optimal channels. Fig. 2A shows a GP sequentially fit on the data from EMG-0, with its max found at channel [1,1] as required. The GP's standard deviation becomes larger (red) as we move away from the training data, reflecting its uncertainty as to how the true function would respond at these faraway points. Fig. 2B shows 2-dimensional slices of the same GP, after several queries.

3) Sequential Optimization: Before any queries are performed, a GP has no information about the system it models. To initialize the sequential optimization process, a volley of random query points must first be made so that BO can efficiently guide exploration. This number of initial random query points is problem-dependent, and is explored in the Results section for our experiments. Once a GP is initialized, we use the Upper Confidence Bound (UCB) acquisition function [10] $\mathrm{UCB}(x) = \mu(x) + k\sigma(x)$ to identify the next query likely to maximize the objective. The parameter k explicitly modulates the trade-off between exploration (high k) and exploitation (low k). The performance of the algorithm is sensitive to this hyperparameter and tuning it by cross-validation or some other method will be necessary for portability across different kinds of neural interfaces. In most of our experiments, $k = 5$ performed best. However, when using an accurate mean prior (sec. II-B.4), sometimes reducing k to a value of 2 performed best, since less exploration is needed. We discuss this in more details in sec. III. The procedure for BO is as follows:

Algorithm 1: Bayesian Optimization

```
Result: Best Stimulation Pattern
Randomly pick m initial random pts and initialize Kernel hyperparameters;
while haven't converged on single stimulation pattern do
    Fit GP to current dataset;
    Compute acquisition function;
    next_stim = max(acq);
    Augment dataset with next_stim;
end
```

Deciding when to stop is an important criterion for online use. Most local numerical optimization procedures, such as gradient descent, set an hyper-parameter ϵ, and stop when the improvement between two steps is less than ϵ. However, this fails for global optimization, in which long-range exploratory queries are necessary. It is possible to use a similar criterion which stops if the improvement of the GP's mean has not improved anywhere, but we find that the simplest and most robust way is to stop after BO has converged on a point. More formally, we set a hyper-parameter t (typically $t = 5$), and stop once BO has been querying the same point t times in a row. However, as the goal of this paper is to outline the efficacy of our algorithm's optimum convergence, it is compared to standard GP-BO in what follows, and most of experiments are reported with a fixed number of query points (100) to better outline trends.

4) Hierarchical GP: This section describes the main algorithmic contribution of the paper. Our goal, as previously defined, is to find the multi-electrode stimulation pattern with the best response, where best is defined through the objective function C. The challenge here is that the space of spatiotemporal multi-electrode patterns grows exponentially in the number of channels and stimulation events. For two-electrode stimulation on our 2×5 grid for example, there are 100 combinations of channel pairs possible, without even considering different inter-event intervals Δt. The direct approach of training a GP directly on this space is not scalable, and does not take advantage of prior knowledge of motor circuit coding; namely, that motor outputs can often be decomposed (although not exactly) into individual neural-muscle correspondences [12]. We leverage this fact in a hierarchical approach where we use GPs fitted on lower dimensional stimuli spaces, to build priors for GPs in higher dimensional stimuli spaces.

More formally, for the two-electrode space $s_2 = (c_1, c_2, \Delta t)$, with single-electrode GP written as $f_1(c) \sim \mathrm{GP}(0, K_1)$, the prior for the two-electrode GP is

$$f_2(c_1, c_2, \Delta t) \sim \mathrm{GP}(a_1 \bar{f}_1^n(c_1) + a_2 \bar{f}_1^n(c_2), K_2) \tag{2}$$

where $f_1^n := f_1|\mathrm{Data}$ is the GP trained on the single-electrode data, $\bar{f}_1^n$ is its mean function, and K_2 is the standard Matern52 [11] multiplicative kernel which separates over

time and space: $K_2\left((c_1^{(1)}, c_2^{(1)}, \Delta t^{(1)}), (c_1^{(2)}, c_2^{(2)}, \Delta t^{(2)})\right) = K_s\left((c_1^{(1)}, c_2^{(1)}), (c_1^{(2)}, c_2^{(2)})\right) K_t\left(\Delta t^{(1)}, \Delta t^{(2)}\right)$.

In summary, the mean prior $a_1 \bar{f}_1^n(c_1) + a_2 \bar{f}_1^n(c_2)$ is constructed by using an independent and additive contribution from the two channels, factoring in the time delay Δt, which is also an explored/optimized parameter. The kernel K_2 is used to learn and correct the multiplicative, nonlinear difference from this prior. The weights a_1 and a_2 and the kernel hyperparameters are optimized incrementally using BO after each new query. The same procedure can be recursively used to include more electrodes, although we present results only for the two-electrode case in this paper. We show in the next section that important gains are obtained from using our method.

III. Results

The main goal of this paper is to provide a proof-of-concept, and to show that Bayesian Optimization algorithms afford a viable and scalable approach to automate neurostimulation tuning. Here, we present basic experimental results on a single monkey, but several EMG readouts, thoroughly verified with exhaustive ground truth that demonstrates the efficacy of our method. Three sets of experimental GP fits are performed. Section III-A reports GP fits on single stimulation event space with single EMG targets. Section III-B reports GP fits on double stimulation event space, using a fixed inter-event interval Δt, still with single EMG targets. Section III-C reports GP fits on double stimulation event space, also optimizing over Δt, with precise multi-EMG coactivation targets.

A. Single Stimulation Event – Single EMG

We start with a thorough analysis of the single-event, single EMG stimulation space using standard GP-BO. This provides a basis for convergence times (in terms of number of initial random points and actively queried points) and allows the introduction of distinct metrics and visualization methods. This step is crucial to our hierarchical method, as the GPs fitted here will serve as building blocks for the ones fitted on more complex spatiotemporal stimulation spaces.

Fig. 2C shows the mean accuracy of the GP's identification of the optimal electrode to stimulate in order to maximize response of EMG-0, as a function of active query points selected by the acquisition function. Prediction accuracy is 1 if the correct best channel was predicted and 0 otherwise, and the reported mean is taken over 25 independent runs where initialization points are randomly selected. Clearly, the number of random initialization query points influences the GP's performance, with more initialization points yielding better prediction, on average. The relation between accuracy and the number of initial query points is further outlined in Fig. 2D. It is worth noting that the number of initial random points appears to be crucial. With certain "bad" initial random points (roughly 25% of the time for the runs using only 5 random initial points), we cannot compensate for a bad initialization by having sequential query points. This is shown by the blue trace in Fig. 2C plateauing at 75%. In other words, for this EMG, having fewer than 35 query points implies hindered convergence on average. Similar behaviors are observed across all tested EMGs (see as another example Appendix Fig. 6). The astute reader may note that Fig. 2C seems to suggest random queries are sufficient, and active queries unnecessary, to achieve good performance in our example. We refer the reader to Fig. 7 in the Appendix that demonstrates the added benefits of active querying by reporting statistics over several trials and multiple EMGs. Moreover, we expect this benefit to grow for larger search spaces; it is not surprising that random querying performs well on a 2×5 grid. Importantly, as is shown below, active querying in single-event GP have a marked impact on hierarchical GP performance.

Indeed, the point of these single event, single muscle GPs, is to use them as priors for higher dimensional GPs. As such, their utility comes from reducing the more complex search spaces, which does not necessarily require predicting the best channel correctly for single EMGs. For example, many channels could be close to the max (see for example Fig. 3A), and as long as the lower dimensional GP predicts a high enough value for them, the higher dimensional GP will be able to test their combinations and find the best stimulation pattern. For this reason, what matters is the value predicted at the optimal channel, not whether it is the max among all of the channels. As long as it is not too far off, the higher dimensional GP will be able to learn the correction term. Fig. 2E shows performance as in Fig. 2D in terms of $l_{\max}$ distance:

$$l_{\max}(f, \text{data} = \{r(s_k)\}) = |\max_{s_k} f(s_k) - \max_{s_k} \mathbb{E}[C(r(s_k))]|$$

where f is the GP mean. We use this measure of distance because it captures the prediction at the max channel which interests us, and not how well the GP is modeling the true function at other (lower response) points. We are making the assumption (Eq.2) that the most responsive stimulation pattern will contain the most responsive single channel stimulation. Any divergence from this prior will have to be found by the nonparametric part of the GP.

Similarly to the trend mean accuracy reveals, the distance metric gets progressively smaller as more sequential points are actively queried (left to right), and also decreases with the addition of initial random points. With just 45 random and 40 sequential points ("O" annotation in Fig. 2E), less than half the number of points in the dataset (200 in total), $l_{\max}$ distance drops to 0.0009. This consists of a 6% ($1 - \frac{0.0139-0.0009}{0.0139}$) error in maximal EMG output, over 25 GP fits, which is negligible. Importantly, the diagonal marked with "D" in Fig. 2E, denoting a total of 55 query points, already has a negligible error (between 0.001 and 0.003 in $l_{\max}$, representing a $7-21\%$ error). Even more surprising, we show below that we only need about 25 total query points on average, 15 random and 10 actively queried ("x" annotation in Fig. 2E), to build a good enough prior for the higher dimensional stimulation spaces.

B. Two Stimulation Events – Single EMG (Fixed Δt)

Toward our goal to evoke targeted muscle co-activations, we start with a minimal setting in which the hierarchical

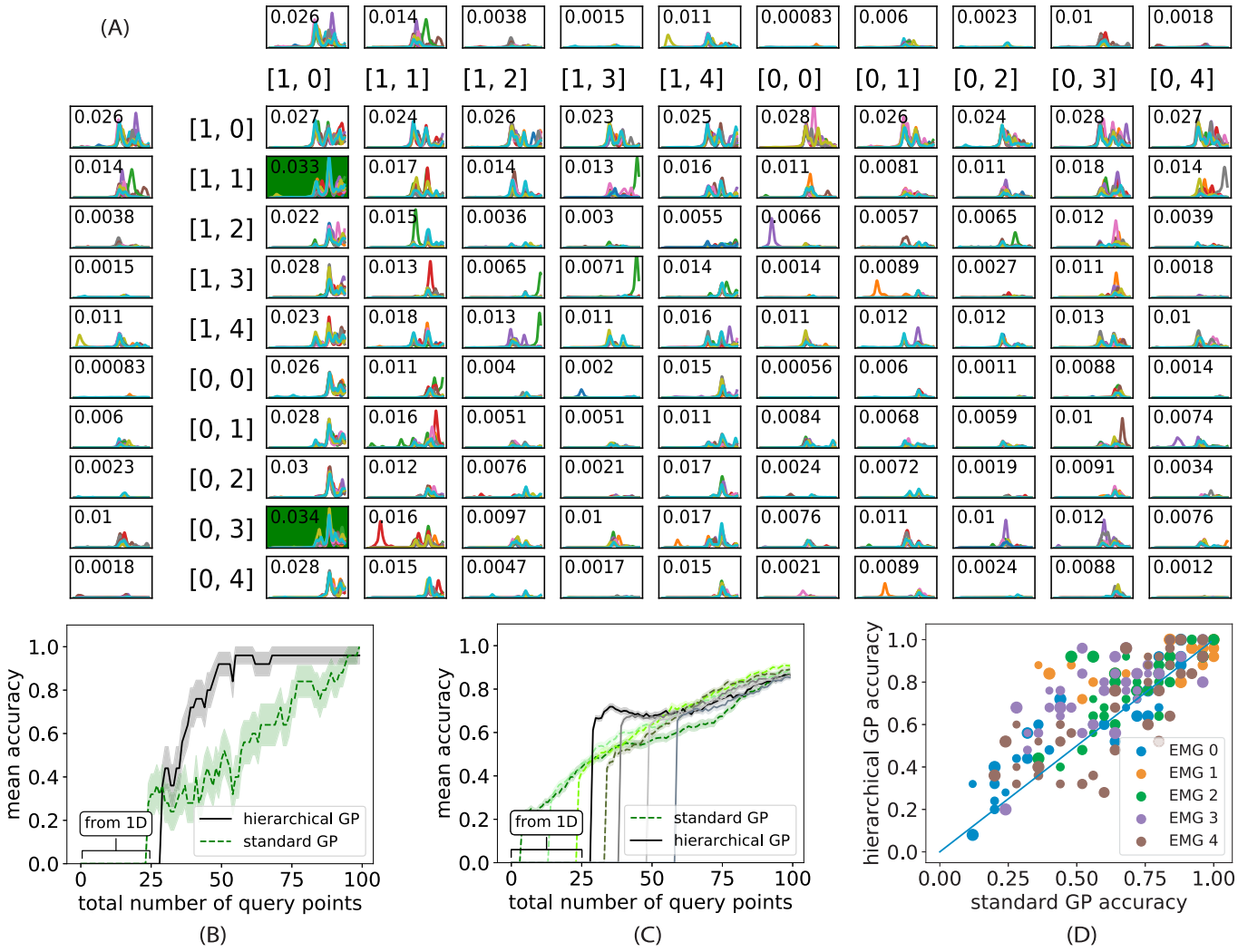

Fig. 3. (A) Search space of EMG-4 responses to double-event stimulation with $\Delta t = 60$ms. First stimulated channel coordinate listed vertically, and second horizontally. For comparison, side and top plots show single stimulation event responses for corresponding channel. Different color lines indicate responses on different stimulation trials (n=10). Average max responses are displayed on the plots, with green cells denoting best stimulations. (B) Mean Prediction accuracy vs. total number of queries comparing our approach to a standard GP for EMG-4. Mean and standard deviation (shaded area) sampled over 10 independent fits. Best performance for standard GP uses 25 random initialization points (shown). Hierarchical GPs uses only 5 random initialization points followed by 25 BO updates in single stimulation event space (1D) before their use as priors for initializing GP in double stimulation event space. (C) Mean GP prediction accuracy over 10 independent fits of all 5 recorded EMGs and Δt pairs. Shaded area shows standard error of the mean of all trials for all muscles. Distinct curves designate distinct numbers of random initialization points (5,10,25,35) apparent from departure from x-axis. Hierachical GPs use 25 BO queries in 1D. (D) Scatter plot of the mean accuracy for our GP model v.s. standard GP for equal number of total query points. Same data as in B. Color indicates muscle number, marker size indicates number of query points used. Blue line indicates identity ($x = y$).

approach is useful: finding the optimal double event stimulation, with fixed inter-event interval Δt, to maximally evoke a single EMG response. Fig. 3A shows the exhaustive search space of dual channel stimulation for an example EMG (*opponens pollicis*, EMG-4), with the mean maximal response over 10 trials displayed in the plots. We refer the reader to the Appendix (Figs. 9,11,13) for search space plots of other EMGs.

Interestingly, for EMG-4, the linear additive prior (eq. 1) predicts stimulating channel [1,0] twice to generate the highest response, however we see that nonlinear effects are such that "priming" by first stimulating either channel [1,1] or channel [0,3], and then following with channel [1,0], yields the highest mean response. Because both of these patterns lead to extremely similar responses, we accept finding either of them as being accurate when comparing algorithms in what follows.

Because this space is our final objective in this experiment, our goal is to achieve a high performance level for prediction accuracy. Fig. 3B shows mean accuracy (over 10 independent fits) with respect to the total number of query points used, for both a standard GP and our hierarchical GP. The later used 25 query points to first fit a model to single stimulation event EMG responses, shown by the labeled offset in Fig. 3B. Both models use the same number of random initial query points (5) and small changes to this number did not qualitatively affect our results. Observe that, even for such a small search space of 100 possible stimulation patterns, first spending 25 queries to build a mean prior using single event

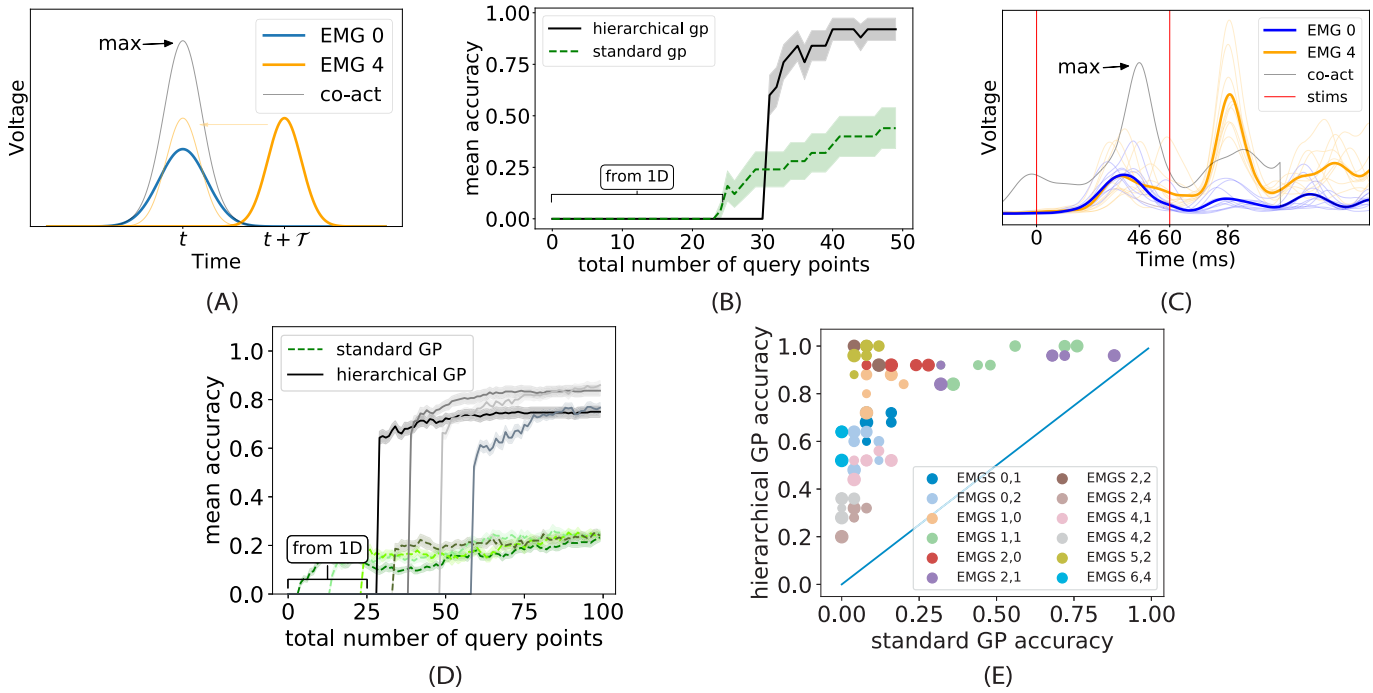

Fig. 4. (A) Temporal co-activation target for objective function. To get a scalar objective, we translate r_4 by τ, sum the responses and take the max. Eq. (3). (B) Mean Prediction accuracy vs. total number of queries comparing our approach to a standard GP for co-activation of EMGs 0 & 4 with $\tau = 40$ms. Mean and standard deviation (shaded area) sampled over 10 independent fits. Best performance for standard GP uses 25 random initialization points (shown). Hierarchical GPs uses only 5 random initialization points followed by 25 BO updates in 1D. (C) Temporal co-activation, as described in C, found by our method. Thin colored lines show individual muscle responses on 10 distinct trials. Thick lines show mean response. Grey line shows summed translated means, as in A. Red lines show the two stimulation times. (D) Mean GP prediction accuracy over 12 co-activated muscle pairs with $\tau = 40$ms. GPs are optimized over all double-event channel pairs, and all inter-event intervals Δt. Mean was computed over 10 independent fitss for each co-activation target. Shaded area shows standard error of the mean of all trials for all co-activations. Distinct curves designate distinct numbers of random initialization points (5,10,25,35) apparent from departure from x-axis. In all cases, hierachical GPs use 25 BO queries in 1D (E) Scatter plot of mean accuracy of our GP model v.s. standard GP, for equal number of query points. Same data as in A. Color indicates co-activation muscle pair, marker size indicates number of query points used to obtain reported accuracy. Blue line indicates identity ($x = y$).

stimulation is worthwhile. This advantage can only grow as the space of stimulation patterns increases in dimensions.

To validate this finding, we conduct an extensive comparison of the two algorithms over all recorded EMGs, and report mean accuracy over 10 independent GP fits for each of the five EMGs, and for each Δt value considered (but still fixed). For a fair comparison, we perform these experiments for four distinct numbers of random initialization points (5,15,25,35) for both the standard GP-BO, and our algorithm. Fig. 3C reports the mean and standard deviation of these ensembles of fits, with respect to the number of query points used. In such a simple search space, although the hierarchical GP has a quicker start, both methods reach similar performance, given enough query points. This is due to the fact that several EMGs have their optimal stimulation patterns being the double stimulation of the same channel, which is a case easily solved by the standard GP. Nevertheless, the scatter plot in Fig. 3D shows that for equal number of query points, our hierarchical GP most often performs better than a standard GP. We see below that the marked advantage of our approach resides in EMG coactivation targets, where distinct EMGs need to be activated at precise times.

C. Two Stimulation Events – EMG Co-Activation Patterns

To reveal the greatest advantage offered by our hierarchical algorithm, we now target temporal co-activation of multiple EMGs, which are likely to require varied and distributed stimulation patterns to evoke. Fig. 4A illustrates such a co-activation, where EMG-0 (*flexor carpi ulnaris*) is required to activate before EMG-4 (*opponens pollicis*) with a 40 ms delay in between peaks. In order to formulate this problem using a similar objective function as described in the Methods section, we define a new objective composed of the appropriately shifted sum of the two EMG activations, and take the maximum of the resulting waveform:

$$C(r(s_2)) = max_t \left[r_0(s_2, t) + r_4(s_2, t + 40) \right]. \qquad (3)$$

This process is illustrated in Fig. 4A.

Equipped with this objective function, we first showcase search results on the specific example outlined above, and then give aggregate statistics over several co-activation targets. For this example, Δt is restricted to the discrete set $(20, 40, 60)$ ms, allowing the interested reader to easily visualize the search space in Appendix Fig. 15). For best results, spatial kernel dimensions share lengthscales which are limited between 1 and 2 so as to avoid spurious local minima where either the data is explained by noise only ($l = \infty$) or the responses become independent ($l = 0$) [11]. Noise standard deviation is also limited between 5e−4V and 1e−3V (typical EMG response size are between 1e−2V and 3e−2V), which encompasses the empirical standard deviation of every stimulation pattern. Fig. 4B compares mean accuracy of a

standard GP directly trained on the two-electrode space, and our GP method, as a function of total query points. Standard GP uses 25 random initialization points while hierarchical GP uses 5 with an additional 25 BO query points to build priors (see offset in Fig. 4B). The mean accuracies are computed over 10 independent fits for each method. Standard GP-BO struggles to reach 50% accuracy while in contrast, our hierarchical method reaches near perfect accuracy after about 40 query points, including the initial 25 queries used to train the GP used for priors in the single stimulation event space. This means that our algorithm converges to the true best stimulation pattern, namely $(c1, c2, \Delta t) = ([1, 1], [1, 0], 60)$, out of a possible 300 (100 channel pairs and 3 time delays Δt) with only 40 total queries. Fig. 4C shows the resulting EMG co-activation found.

To validate the performance revealed by this example target EMG co-activation, performance over 12 distinct EMG co-activation pairs was evaluated. Fig. 4D reports mean accuracy comparisons evaluated over 10 independent fits for each EMG combinations, with GP-BO algorithms searching over all pairs of stimulation channels and all 7 inter-event time intervals. For comparison, fits were performed for four distinct numbers of random initialization points: 5, 15, 25, 35. Although hierarchical GP-BO does not always reach full accuracy (some EMG co-activations tested were difficult to evoke), it largely outperforms standard GP-BO on average. Moreover, the scatter plot in Fig. 4E shows that for equal number of query points, hierarchical GP-BO outperforms standard GP-BO in every case.

IV. Conclusion

We showed that the hierarchical approach to build GPs on the space of multi-electrode stimulation patterns is a viable one to identify optimal inputs for a given target EMG output. Not only does it far outperform the standard GP approach (and random search), it can potentially be used online to find the optimal stimulation strategy for a desired co-activation output. This is a step forward in linking brain activity and behavior by being able to control muscles directly [13], and for the use of neural prostheses to improve motor recovery after stroke or other motor system injuries.

The most novel part of our work is the ability of our algorithm to leverage known properties of single channel neurostimulation into priors to appreciably accelerate search of complex spatiotemporal neurostimulation patterns. As a proof of concept, we used a restricted stimulation search space for which we could exhaustively sample all stimulation combinations, and clearly demonstrated faster learning in thorough offline tests.

V. Discussion

A. Random Query Points for Initialization

EMG responses, not unlike many other biological signals, tend to follow poisson models (see next subsection), where the variance equals the mean. Unfortunately, none of the current standard BO packages provide Poisson likelihood models. One way to circumvent this problem is by asking for more initial random queries. However, how many random points to use at initialization is system dependent and will need to be calibrated based on the use case. It is for this reason we opted to report algorithmic performance for a wide range or random initial queries. We note however that this consideration is only limited to the low-dimensional space used to build priors. Indeed, for higher dimensional models initialized with these priors, no random initialization points are necessary. As this process is iterated in even higher dimensions, the cost of initial random points will diminish.

B. Priors and Hierarchical Kernel Interactions

We made a few simplifying modeling assumptions in our hierarchical kernel interactions, which could be improved upon in future work. For one, we assumed homoscedastic additive Gaussian noise [11], whereas biology is often better described by Poisson noise (see Fig. 1C and Fig. 2), or even more complex models [14]. Second, we trained the GPs for different muscles (for each r_i) independently, whereas they are clearly correlated (see Fig. 1B/C), and could potentially share information through multi-output (also called co-Kriging) models. We did try this approach since it is relatively easy to implement (see [15] for a review), but it proved unnecessary because we record activity on all EMGs for every stimulation. Co-kriging is most effective when two response variables are correlated and one (eg. elevation) is easier to measure than the other (eg. air temperature). Third, using a non-stationary kernel could accelerate the search even more [16]. This would allow using a large lengthscale for most of the search space, yet having a smaller lengthscale near optimal stimulation patterns to permit pinpointing the true maximum.

C. Other Stimulation Modalities

We note that our method can easily be adapted to more complex objective functions such as incorporating both forelimb and hindlimb movements, and to different sensor modalities such as acceleration from an accelerometer or 3D position from cameras. This means that rather than optimizing for high EMG output, we could directly optimize for movement amplitude and direction using, for example, DeepLabCut [17] to get pose estimations. Furthermore, our approach is not confined to cortical microstimulation. Indeed, spinal and peripheral nerve stimulation are promising approaches that could be used to evoke targeted movements, and our hierarchical stimulation optimization is directly applicable to these settings.

Long train stimulations (500ms) have already been shown to evoke complex multi-joint movements [7]. However, we still lack a mechanistic explanation for the role of cortical dynamics in the generation of these movements. We believe that scaling our approach could provide answers by uncovering optimal spatiotemporal stimulation patterns to evoke complex movements. Our preliminary results already show that our algorithm is capable of revealing circuit-level computations, beyond the assumed linear and additive combination used to create priors. This makes it a good scientific tool that can not only be used for pure optimization of a BCI control signal, but also for asking hypothesis-driven questions about the brain.

ACKNOWLEDGMENTS

The authors would like to thank A. Bogaard, E. Fetz, C. Moritz, M. P. Touzel, and O. Caron-Grenier for useful discussions. They also acknowledge the important contributions of S. Quessy for experimental implementations and data collection.

REFERENCES

[1] (2013). *Spinal Cord Injury*. Accessed: Nov. 15, 2018. [Online]. Available: http://www.who.int/news-room/fact-sheets/detail/spinal-cord-injury

[2] A. G. Thrift *et al.*, "Global stroke statistics," *Int. J. Stroke*, vol. 9, no. 1, pp. 6–18, Jan. 2014.

[3] B. A. T. G. P. C. B. Cioni and T. Tufo, "Motor cortex stimulation for movement disorders," *J Neurosurg Sci*, vol. 2, pp. 230–241, Jun. 2016.

[4] N. Wenger *et al.*, "Spatiotemporal neuromodulation therapies engaging muscle synergies improve motor control after spinal cord injury," *Nature Med.*, vol. 22, no. 2, pp. 138–145, Feb. 2016.

[5] A. Selfslagh *et al.*, "Non-invasive, brain-controlled functional electrical stimulation for locomotion rehabilitation in individuals with paraplegia," *Sci. Rep.*, vol. 9, no. 1, Dec. 2019, Art. no. 6782.

[6] P. D. Cheney, D. M. Griffin, and G. M. Van Acker, "Neural hijacking: Action of high-frequency electrical stimulation on cortical circuits," *Neuroscientist*, vol. 19, no. 5, pp. 434–441, Oct. 2013.

[7] M. S. A. Graziano, C. S. R. Taylor, and T. Moore, "Complex movements evoked by microstimulation of precentral cortex," *Neuron*, vol. 34, no. 5, pp. 841–851, May 2002.

[8] A. Hamadjida, M. Dea, J. Deffeyes, S. Quessy, and N. Dancause, "Parallel cortical networks formed by modular organization of primary motor cortex outputs," *Current Biol.*, vol. 26, no. 13, pp. 1737–1743, Jul. 2016, doi: 10.1016/j.cub.2016.04.068.

[9] J. H. Kaas, "Plasticity of sensory and motor maps in adult mammals," *Annu. Rev. Neurosci.*, vol. 14, no. 1, pp. 137–167, Mar. 1991.

[10] E. Brochu, V. M. Cora, and N. de Freitas, "A tutorial on Bayesian optimization of expensive cost functions, with application to active user modeling and hierarchical reinforcement learning," *CoRR*, vol. abs/1012.2599, May 2010.

[11] C. E. Rasmussen and C. K. I. Williams, *Gaussian Processes for Machine Learning* (Adaptive Computation and Machine Learning). Cambridge, MA, USA: MIT Press, 2005.

[12] A. Georgopoulos, A. Schwartz, and R. Kettner, "Neuronal population coding of movement direction," *Science*, vol. 233, no. 4771, pp. 1416–1419, Sep. 1986.

[13] A. P. Alivisatos *et al.*, "Neuroscience. the brain activity map," *Science*, vol. 2, pp. 1284–1285, Feb. 2013.

[14] L. S. Tsimring, "Noise in biology," *Rep. Prog. physics. Phys. Soc.*, vol. 77, no. 2, Feb. 2014, Art. no. 026601. [Online]. Available: https://www.ncbi.nlm.nih.gov/pubmed/24444693

[15] M. A. Álvarez, L. Rosasco, and N. D. Lawrence, "Kernels for vector-valued functions: A review," *Found. Trends Mach. Learn.*, vol. 4, no. 3, pp. 195–266, 2012, doi: 10.1561/2200000036.

[16] J. Snoek, K. Swersky, R. Zemel, and R. Adams, "Input warping for Bayesian optimization of non-stationary functions," *ser. Proc. Mach. Learn. Res.*, vol. 32, no. 2. Bejing, China: PMLR, 22–24 Jun. 2014, pp. 1674–1682. [Online]. Available: http://proceedings.mlr.press/v32/snoek14.html

[17] A. Mathis *et al.*, "DeepLabCut: Markerless pose estimation of user-defined body parts with deep learning," *Nature Neurosci.*, vol. 21, no. 9, pp. 1281–1289, Sep. 2018, doi: 10.1038/s41593-018-0209-y.